10

Design and Applications of Continuous-Time Chaos Generators

Carlos Sánchez-López[1], Jesus Manuel Muñoz-Pacheco[2], Victor Hugo Carbajal-Gómez[3], Rodolfo Trejo-Guerra[4], Cristopher Ramírez-Soto[5], Oscar S. Echeverria-Solis[6] and Esteban Tlelo-Cuautle[7]
[1]*UAT, CSIC and University of Sevilla*
[2]*Universidad Politécnica de Puebla*
[3]*INAOE*
[1,2,3,4,5,6,7]*México*
[1]*Spain*

1. Introduction

Chaos systems can be classified as one type of complex dynamical systems that possess special features such as being extremely sensitive to tiny variations of initial conditions. In general, for deterministic chaos to exists, a dynamical system must have a dense set of periodic orbits, it must be transitive and it has to be sensitive to initial conditions (Strogatz, 2001). Chaos systems have bounded trajectories in the phase space, and they have at least one positive maximum Lyapunov exponent (Dieci, 2002; Lu et al., 2005; Muñoz-Pacheco & Tlelo-Cuautle, 2010; Ramasubramanian & Sriram, 2000).

Nowadays, several chaos generators have been implemented with electronic devices and circuits in order to have a major impact on many novel applications, as the ones reported in (Cruz-Hernández et al., 2005; Ergun & Ozoguz, 2010; Gámez-Guzmán et al., 2008; Lin & Wang, 2010; Strogatz, 2001; Trejo-Guerra et al., 2009). Furthermore, this chapter is mainly devoted to highlight the design automation of continuous-time multi-scroll chaos generators, their implementations by using behavioral models of commercially available electronic devices, their experimental realizations and applications to secure communications. A review of the double-scroll Chua's circuit is also presented along with the generation of hyperchaos by Coupling Two Chua's circuits. Basically, we present the generation of multi-scroll attractors by using saturated nonlinear function series. We show their implementation by using traditional operational amplifiers (opamps) and current-feedback operational amplifiers (CFOAs) (Senani & Gupta, 1998). Besides, we summarize some performances of multi-scroll chaos generators by using opamps (Muñoz-Pacheco & Tlelo-Cuautle, 2010), CFOAs (Trejo-Guerra, Sánchez-López, Tlelo-Cuautle, Cruz-Hernández & Muñoz-Pacheco, 2010), current conveyors (CCs) (Sánchez-López et al., 2010) and unity-gain cells (UGCs) (Sánchez-López et al., 2008). However, not only the CC and the UGC can be taken from the commercially available CFOA AD844, but also they can be designed with standar integrated complementary metal-oxide-semiconductor (CMOS) technology (Trejo-Guerra, Tlelo-Cuautle, Muñoz-Pacheco, Cruz-Hernández & Sánchez-López, 2010).

The usefulness of the chaos generators is highlighted through the physical realization of a secure communication system by applying Hamiltonian forms and observer approach (Cruz-Hernández et al., 2005). This chapter finishes by listing several trends on the implementation of chaos generators by using integrated CMOS technology, which may open new lines for research covering the behavioral modeling, synthesis, design and simulation of integrated chaotic oscillators.

1.1 Description of a chaos system

In order to make any quantitative progress in understanding a system, a mathematical model is required. The model may be formulated in many ways, but their essential feature allows us to predict the behavior of the system, sometimes by given its initial conditions and a knowledge of the external forces which affect it. In electronics, the mathematical description for a dynamical system, most naturally adopted for behavioral modeling, is done by using the so-called state-space representation, which basically consists of a set of differential equations describing the evolution of the variables whose values at any given instant determine the current state of the system. These are known as the state variables and their values at any particular time are supposed to contain sufficient information for the future evolution of the system to be predicted, given that the external influences (or input variables) which act upon it are known.

In the state-space approach, the differential equations are of first order in the time-derivative, so that the initial values of the variables will suffice to determine the solution. In general, the state-space description is given in the form:

$$\begin{aligned} \dot{\mathbf{x}} &= \mathbf{f}(\mathbf{x}, \mathbf{u}, t) \\ \mathbf{y} &= \mathbf{h}(\mathbf{x}, \mathbf{u}, t) \end{aligned} \tag{1}$$

where the dot denotes differentiation with respect to time (t) and the functions $\mathbf{f}$ and $\mathbf{h}$ are in general nonlinear. In (1), the variety of possible nonlinearities is infinite, but it may nevertheless be worthwhile to classify them into some general categories. For example: There are simple analytic functions such as powers, sinusoids and exponentials of a single variable, or products of different variables. A significant feature of these functions is that they are smooth enough to possess convergent Taylor expansions at all points and consequently can be linearized (Strogatz, 2001). A type of nonlinear function frequently used in system modeling is the piecewise-linear (PWL) approximation, which consists of a set of linear relations valid in different regions (Elhadj & Sprott, 2010; Lin & Wang, 2010; Lü et al., 2004; Muñoz-Pacheco & Tlelo-Cuautle, 2009; Sánchez-López et al., 2010; Suykens et al., 1997; Trejo-Guerra, Sánchez-López, Tlelo-Cuautle, Cruz-Hernández & Muñoz-Pacheco, 2010; Yalçin et al., 2002). The use of PWL approximations have the advantage that the dynamical equations become linear or linearized in any particular region, and hence the solutions for different regions can be joined together at the boundaries.

When applying PWL approximation to a system described by (1), the resulting linearized system has finite dimensional state-space representation, as a result the equations describing a linear behavioral model become:

$$\begin{aligned} \dot{\mathbf{x}} &= \mathbf{A}\mathbf{x} + \mathbf{B}\mathbf{u} \\ \mathbf{y} &= \mathbf{C}\mathbf{x} + \mathbf{D}\mathbf{u} \end{aligned} \tag{2}$$

where **A, B, C**, and **D** are matrices (possibly time-dependent) of appropriate dimensions. The great advantage of linearity is that, even in the time dependent case, a formal solution can

immediately be constructed, which is moreover applicable for all initial conditions and all input functions.
An important point which must be kept in mind for a nonlinear dynamical system, is that the stability properties are essentially more complicated than in the linear case. For instance, when nonlinearities are present, several features can appear such as limit cycles or the phenomenon known as chaos (Chakraborty & Dana, 2010; Chua, 1975; Cook, 1994; Muñoz-Pacheco & Tlelo-Cuautle, 2010; Ott, 1994; Strogatz, 2001).

1.2 Autonomous systems

Although the equations describing a behavioral dynamical model will in general depend on the time, either explicitly or through the input function, or both, a large part of nonlinear system theory is concerned with cases where there is no time dependence at all (Ott, 1994). Such systems are said to be autonomous, and they arise quite naturally in practice when, for example, the input vector is held fixed. In any such case, the differential equation for the state vector become:

$$\dot{\mathbf{x}} = \mathbf{f}(\mathbf{x}, \hat{\mathbf{u}}) \tag{3}$$

where $\hat{\mathbf{u}}$ is a constant vector. Thus, the equilibrium points in the state-space are determined by $\mathbf{f}(\mathbf{x}, \hat{\mathbf{u}}) = 0$. Assuming that $\mathbf{f}(\mathbf{x}, \hat{\mathbf{u}})$ satisfies Lipschitz condition (Chua, 1975), the differential equation for $x(t)$ will have a unique solution, for any given initial state $x(0)$. The path traced out in the state-space by $x(t)$ is called a trajectory of the system and because of the uniqueness property, there will be one and only one trajectory passing through any given point. If it is suppressed the dependence on $\hat{\mathbf{u}}$, the state-space differential equations for an autonomous system can be written simply as:

$$\dot{\mathbf{x}} = \mathbf{f}(\mathbf{x}) \tag{4}$$

and the set of all trajectories of this equation provides a complete geometrical representation of the dynamical behavior of the system, under the specified conditions. As a result, it is possible to give an essentially complete classification of behavior in the phase plane, though not in higher-dimensional state-spaces. In general, the equations describing a nonlinear system cannot be solved analytically, so that, in order to construct the trajectories accurately, it is necessary to use numerical methods.

1.3 Strange attractors and chaos

Although singular points and closed curves constitute the only asymptotic terms of bounded trajectories for autonomous systems in the phase plane, this is no longer true in spaces of higher dimension (Cook, 1994). In general, the term for a limit set where all trajectories in its vicinity approach it as $t \to \infty$; is an attractor, since it asymptotically attracts nearby trajectories to itself. For second-order dynamical systems, the only types of limit set normally encountered are singular points and limit cycles. Consequently, a continuous-time autonomous system requires more than two dimensions to exhibit chaos (Cook, 1994; Ott, 1994; Strogatz, 2001). More complicated still are the so-called strange limit sets (Strogatz, 2001). They may or may not be asymptotically attractive to neighboring trajectories; if so, they are known as strange attractors, though even then, the trajectories they contain may be locally divergent from each other, within the attracting set. Such structures are associated with the quasi-random behavior of solutions called chaos (Cook, 1994).

2. Chua's circuit and Hyperchaos

Over the last two decades, theoretical design and circuit implementation of various chaos generators have been a focal subject of increasing interest due to their promising applications in various real-world chaos-based technologies and information systems (Cook, 1994; Cruz-Hernández et al., 2005; Ergun & Ozoguz, 2010; Gámez-Guzmán et al., 2008; Lin & Wang, 2010; Ott, 1994; Strogatz, 2001; Trejo-Guerra et al., 2009).
In electronics, among the currently available chaotic oscillators, Chua's circuit has been the most used one (Chakraborty & Dana, 2010; Elhadj & Sprott, 2010; Sánchez-López et al., 2008; Senani & Gupta, 1998; Suykens et al., 1997; Trejo-Guerra et al., 2009), because it can be easily built, simulated, and tractable mathematically. It consists of five circuit elements: one linear resistor, one inductor, two capacitors, and one nonlinear resistor known as Chua's diode (Tlelo-Cuautle et al., 2006).

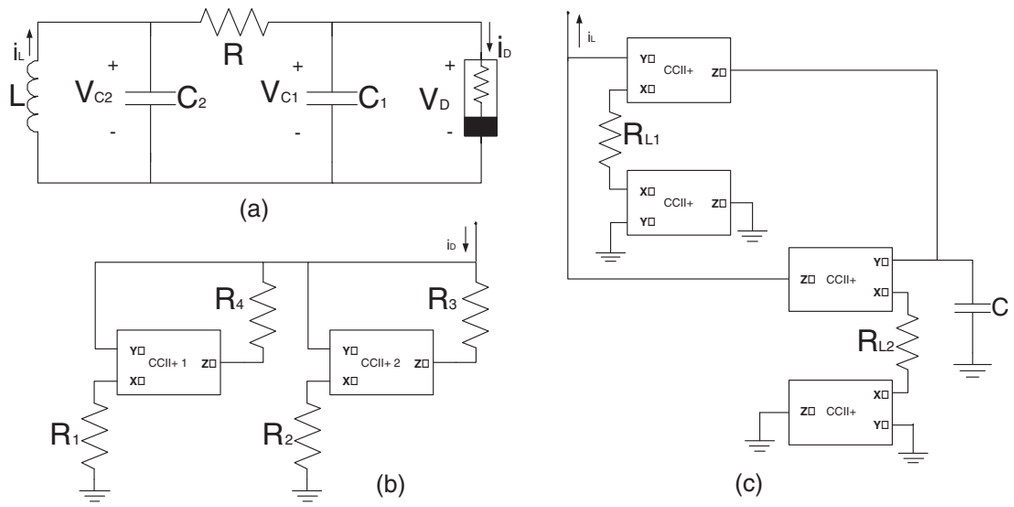

Fig. 1. (a) Chua's circuit, (b) Chua's diode and (c) Simulated inductance using CCII+s.

From the design point of view, there are many ways to realize the inductor and Chua's diode by using electronic devices, e.g. by using current-feedback operational amplifiers (CFOAs) (Senani & Gupta, 1998), positive-type second generation current conveyors (CCII+), and unity-gain cells (UGCs) (Sánchez-López et al., 2008). All these realizations can be made by using the commercially available CFOA AD844 from analog devices. In this subsection we show the realization using CCII+s, which is embedded into the CFOA AD844. It is worthy to mention that current conveyors present nonideal characteristics (Sánchez-López et al., 2010), and since its introduction in 1970 (Sedra & Smith, 1970), recently there exists other topologies (Tlelo-Cuautle & C. Sánchez-López, 2010). Among them, the CCII+ is a very useful building block (Trejo-Guerra et al., 2009).
In Chua's circuit the inductor can be implemented from the gyrator description (Sánchez-Sinencio & Silva-Martínez, 2000), and it can be designed using CCII+s. Chua's diode can also be implemented by using CCII+s as shown in Fig. 1, each CCII+ in Fig. 1(b) is biased with different voltage bias levels: CCII+1 is biased with +5V and CCII+2 with +12V. The values of the resistors are: R_1=6.76$k\Omega$, R_2=3.91$k\Omega$, R_3=470Ω, and R_4=10$k\Omega$. The CCII+ based simulated inductance is shown in Fig. 1(c), where for C=4.7nF, then R_{L1}=R_{L2}=2.36$k\Omega$.
By setting C_1=4.7nF and C_2=47nF in Chua's circuit, and by replacing Chua's diode and the inductor with the proposed circuits shown in Fig. 1(b) and Fig. 1(c), respectively, the sequence

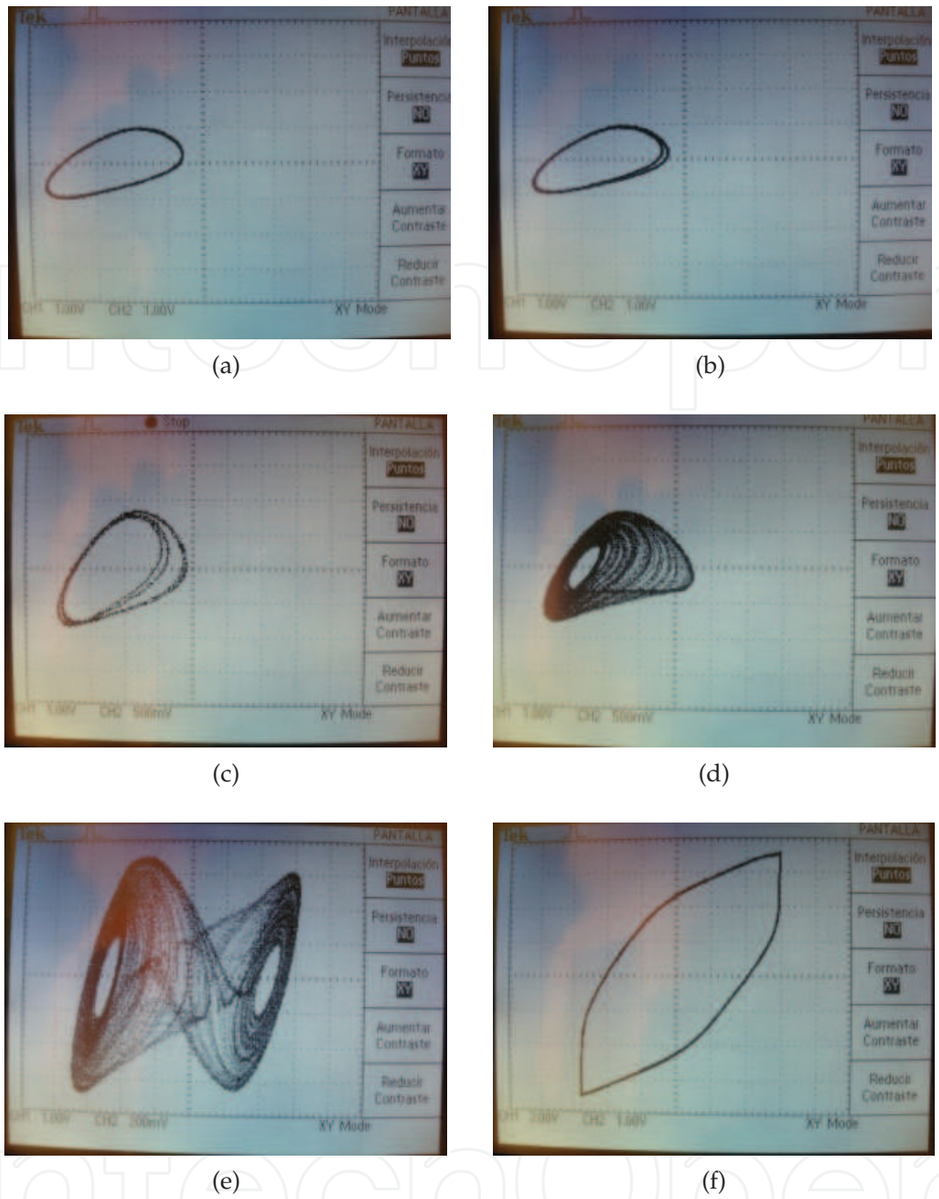

Fig. 2. Sequence of chaotic behaviors from the experimental realization of Chua's circuit

of chaotic behaviors (V_{C1} vs. V_{C2}) are shown in Fig. 2. When R=3490Ω one cycle is observed, with R=3466Ω two cycles, with R=3338Ω four cycles, with R=3261Ω one scroll and with R=2771Ω the double scroll is observed. Finally, the limit cycle is appreciated when R=2712Ω.

2.1 Hyperchaos

Hyperchaos can be generated by coupling two Chua's circuits as shown in Fig. 3. The Chua's circuit in the top of Fig. 3 is composed of RM, C1M, C2M, Chua's diode is implemented with the CCII+s 1DM and 2DM (including R1M to R4M), and the simulated inductance is implemented by C3M and two transconductors realized with two CCII+s (R5M connected between the CCII+s 3LM and 4LM, and R6M connected between the CCII+s 5LM and 6LM).

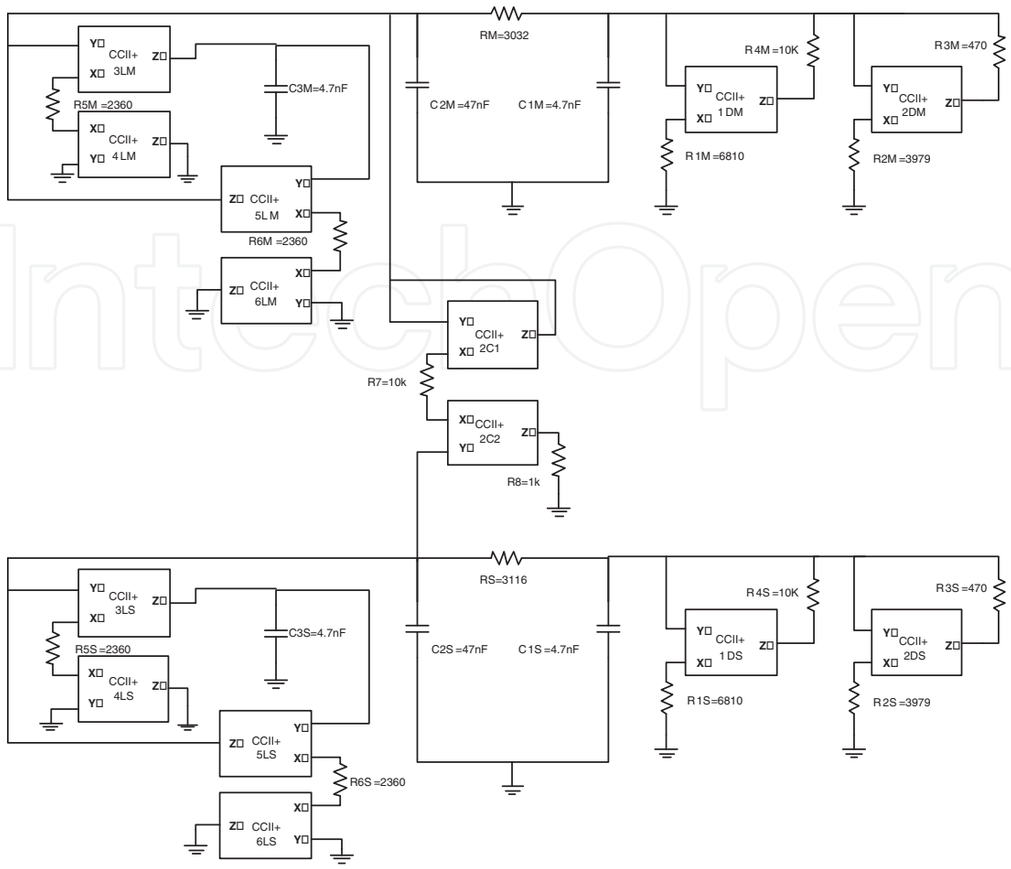

Fig. 3. Coupling two CCII+ based Chua's circuits

The second Chua's circuit (bottom of Fig. 3), is composed of RS, C1S, C2S, Chua's diode is implemented with the CCII+s 1DS and 2DS (including R1S to R4S), and the simulated inductance is implemented by C3S and two transconductors realized with two CCII+s (R5S connected between the CCII+s 3LS and 4LS, and R6S connected between the CCII+s 5LS and 6LS). Finally, the coupling is performed through R7 connected between two CCII+s (2C1 and 2C2). As one sees, RM=3032Ω in the first Chua's circuit has a different value compared to RS=3116Ω in the second Chua's circuit, the rest of the elements in both Chua's circuits have the same value. This difference is attributed to the coupling circuit, in which R7 establishes the gain and it can be varied.

The hyperchaotic behaviors can be appreciated by varying the gain, i.e. R7. In Fig. 4 are shown the hyperchatic behaviors by diminishing R7 without persistence, while in Fig. 5 are shown the same hyperchaotic behaviors provided in Fig. 4 but with persistence. It can be appreciated that hyperchaos is disappearing when R7 is diminished. However, we have a wide range of values for R7 to tune the hyperchaotic behavior for a specific application, e.g. secure communications.

3. Design automation of multi-scroll chaos generators

The design of multi-scroll chaotic attractors can be performed via PWL functions (Elhadj & Sprott, 2010; Lin & Wang, 2010; Lü et al., 2004; Muñoz-Pacheco & Tlelo-Cuautle, 2009; 2010;

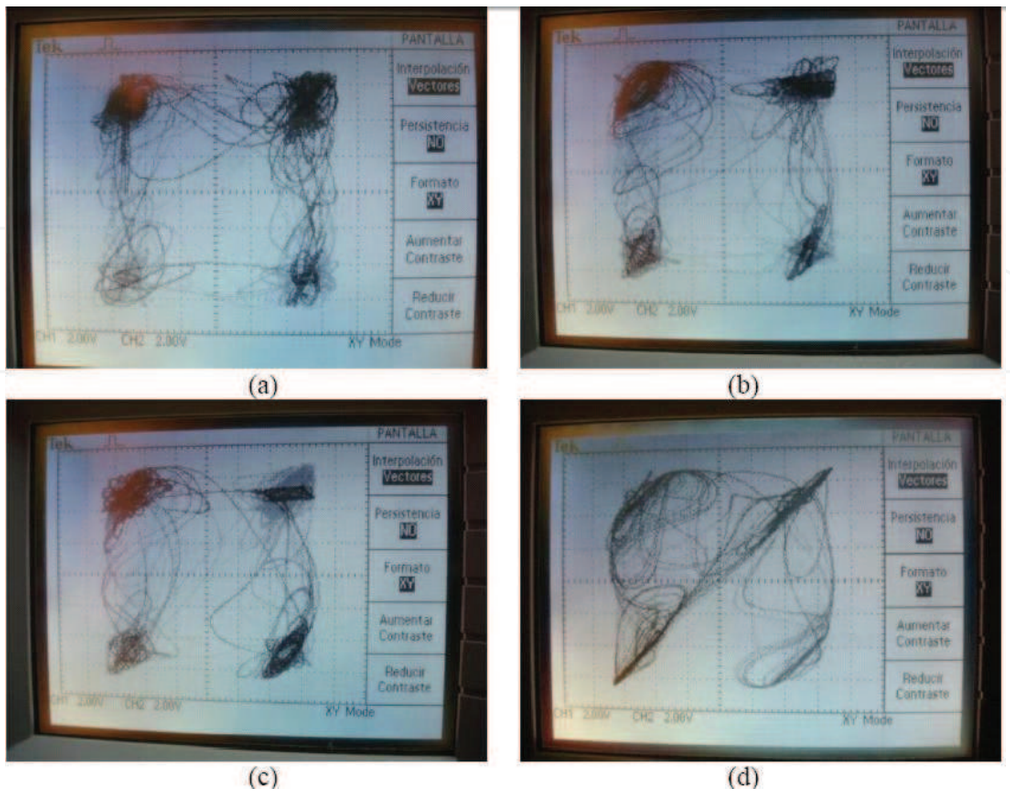

Fig. 4. Hyperchaos with: (a) R7=10kΩ, (b) R7=7kΩ, (c) R7=5kΩ, and (d) R7=500Ω without persistence.

Sánchez-López et al., 2010; Suykens et al., 1997; Trejo-Guerra, Sánchez-López, Tlelo-Cuautle, Cruz-Hernández & Muñoz-Pacheco, 2010; Trejo-Guerra, Tlelo-Cuautle, Jiménez-Fuentes & Sánchez-López, 2010; Yalçin et al., 2002). In the case of Chua's circuit based oscillators, the PWL function is designed by introducing additional breakpoints to Chua's diode (Trejo-Guerra, Sánchez-López, Tlelo-Cuautle, Cruz-Hernández & Muñoz-Pacheco, 2010), or by generalizing Chua's circuit as proposed in (Suykens et al., 1997; Yalcin et al., 2000).

When implementing multi-scroll chaos generators with electronic devices, it is necessary to remark that it is quite difficult to generate attractors with a large number of scrolls due to the limitation of the real dynamic range of the physical devices. Furthermore, among the basic circuits used to generate multi-scroll generators, the step circuit, hysteresis circuit and saturated circuit are the three most used ones. To generate multidimensional multi-scroll attractors, such as 1-D (Yalçin et al., 2002), 2-D (Muñoz-Pacheco & Tlelo-Cuautle, 2009), 3-D (Deng, 2007), and 4-D (Varrientos & Sanchez-Sinencio, 1998), the state equations of this family of systems depends on the number of nonlinear functions, for example: three nonlinear functions are needed to generate 3D-scrolls.

In (Lü et al., 2004) a saturated multi-scroll chaotic system based on saturated function series, is introduced. That system can produce three different types of attractors, as follows: 1-D saturated n-scroll chaotic attractors, 2-D saturated $n \times m$-grid scroll chaotic attractors and 3-D saturated $n \times m \times l$-grid scroll chaotic attractors, where n, m and l are integers and can have the same values. Since this multi-scroll system can be designed by using PWL functions, it is

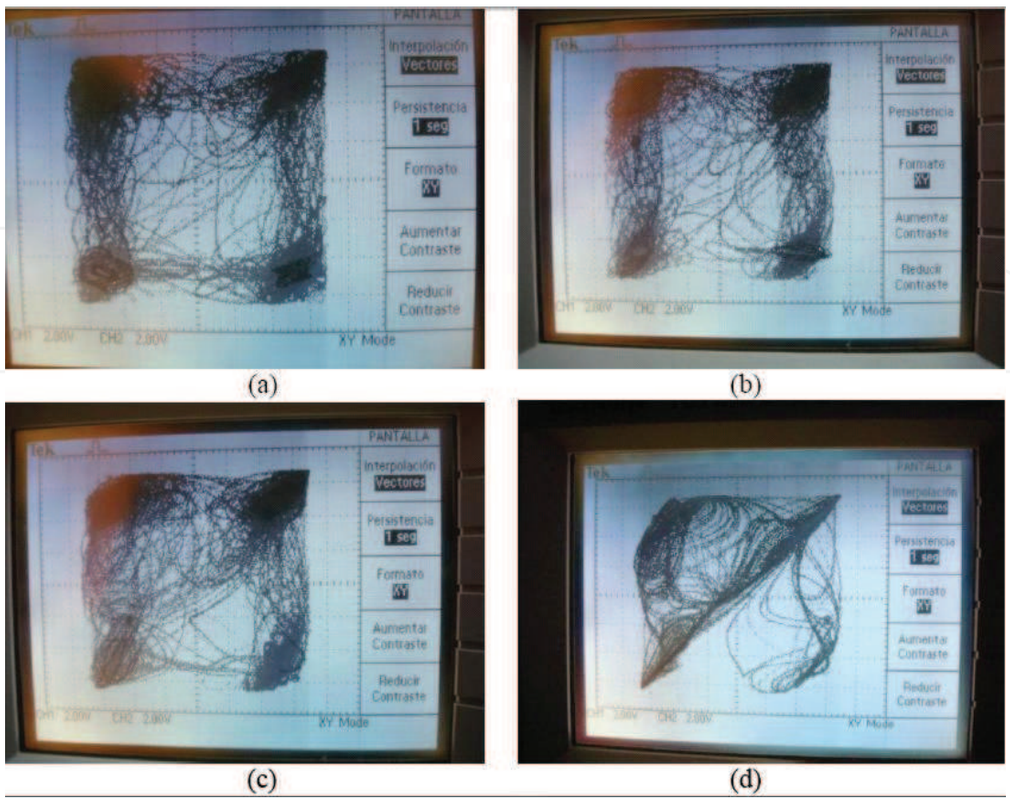

Fig. 5. Hyperchaos with: (a) R7=10kΩ, (b) R7=7kΩ, (c) R7=5kΩ, and (d) R7=500Ω with persistence.

a good chaos system suitable for the development of a systematic design automation process by applying behavioral modeling (Muñoz-Pacheco & Tlelo-Cuautle, 2010).

3.1 Design automation by behavioral modeling

Behavioral modeling can be a possible solution for successful development of analog electronic design automation (EDA) tools, because various types of systems that can be represented by means of an abstract model. The abstraction levels are an indication of the degree of detail specified about how the function is to be implemented. Therefore, behavioral models try to capture as much circuit functionality as possible with far less implementation details than the device-level description of the circuit (Kundert, 2004). However, it is difficult to make a strict distinction between different abstraction levels for analog systems, in contrast to common practice in digital synthesis methodologies (Castro-López et al., 2006). Instead, a division should be made between a description level and an abstraction level. A description level is a pair of two sets: a set of elementary elements and a set of interconnection types. The abstraction level of a description is the degree to which information about non-ideal effects or structure is neglected compared to the dominant behavior of the entire system.

In this manner, whereas a description level indicates how the analog system is represented; an abstraction level deals with the relation between the model of the system and its real behavior. Although it can be clear to consider the functional level at a high abstraction level and the physical level at a low abstraction level, it is not straightforward to compare the abstraction levels of different description levels. Besides, an electronic system can be designed by

converting the functional specification at the highest abstraction level to a physical realization at the lowest abstraction level via operations between description and abstraction levels. Four fundamental types of such operations are distinguished: refinement, simplification, translation and transformation. Simplification is the reverse operation of refinement.
Model generation consists in applying multiple simplification operations to a system representation to obtain a model with less accuracy, but easier to interpret or to simulate. From this point of view, the design automation of an electronic system must indicate the kind and order of the operations to be applied during the design process and must include an appropriate modeling strategy to determine how a system is represented. In fact, the selection of a good modeling strategy makes easier to execute the design process. In (Muñoz-Pacheco & Tlelo-Cuautle, 2010) it is presented the analog design automation process of chaos systems which are modeled from the highest level of abstraction by applying state variables approach and PWL approximations.
For the design of autonomous chaos systems, their state variables approach are defined by (4), where the function **f** is nonlinear. However, the PWL approximation can be used to describe this nonlinear function, which consists of a set of linear relations valid in different regions. Such functions are not analytic at all points, since they contain discontinuities of value or gradient, but they have the advantage that the dynamical equations become linear (and hence soluble) in any particular region, and the solutions for different regions can then be joined together at the boundaries. Furthermore, (4) can be described by the linear state-space representation given in (2). The great advantage of linearity is that, even in the time dependent case, a formal solution can immediately be constructed, which is moreover applicable for all initial conditions and all input functions. A repertoire of the design automation of 1-D, 2-D and 3-D multi-scroll chaos generators by behavioral modeling and realized by using traditional operational amplifiers (opamps), is presented in Muñoz-Pacheco & Tlelo-Cuautle (2010). The chaos generators are based on saturated nonlinear function (SNLF) series, and realized with opamps working in the saturation regions, so that they can be modeled by PWL functions.
In Fig. 6 is shown a SNLF with 5 and 7 segments to generate 3 and 4 multi-scrolls, respectively. In (5) is described the PWL approximation called series of a SNLF, where $k \geq 2$ is the slope of the SNLF and multiplier factor to saturated plateaus, $plateau = \pm nk$, with n=integer odd to even-scrolls and n=integer even to odd-scrolls. h=saturated delay of the center of the slopes in Fig. 6, and must agree with $h_i = \pm mk$, where $i = 1, \ldots, [(scrolls - 2)/2]$ and $m = 2, 4, \ldots, (scrolls - 2)$ to even-scrolls; and $i = 1, \ldots, [(scrolls - 1)/2]$ and $m = 1, 3, \ldots, (scrolls - 2)$ to odd-scrolls; p and q are positive integers.

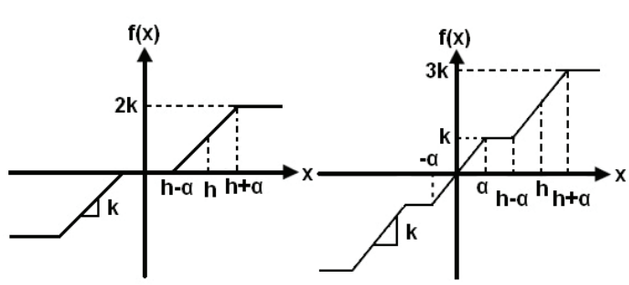

Fig. 6. PWL description of a SNLF with 5 and 7 segments

$$f(x;k,h,p,q) = \sum_{i=-p}^{q} f_i(x;h,k) \tag{5}$$

To generate multi-scrolls attractors a controller is added as shown in (6), where $f(x;k,h,p,q)$ is defined by (7), and a,b,c,d are positive constants and must be $0 < a,b,c,d < 1$ to accomplish chaos conditions (Lü et al., 2004).

$$\begin{aligned} \dot{x} &= y \\ \dot{y} &= z \\ \dot{z} &= -ax - by - cz - df(x;k,h,p,q) \end{aligned} \tag{6}$$

$$f(x;k,h,p,q) = \begin{cases} (2q+1)k & \text{if } x > qh+1 \\ k(x-ih)+2ik & \text{if } \mid x-ih \mid \leq 1 \\ & -p \leq i \leq q \\ (2i+1)k & \text{if } ih+1 < x < (i+1)h-1 \\ & -p \leq i \leq q-1 \\ -(2p+1)k & \text{if } x < -ph-1 \end{cases} \tag{7}$$

The simulation of multi-scrolls attractors modeled by (6) and (7), is executed using (Tlelo-Cuautle & Munoz-Pacheco, 2007). 6-scrolls attractors are generated with a=b=c=d=0.7, k=10, h=20, p=q=2, as shown in Fig. 7. As one sees, Fig. 7a shows that the dynamic ranges (DRs) are very large. Since real electronic devices cannot handle these DRs, (7) cannot be synthesized and it cannot have small DRs because $k \geq 2$ (Lü et al., 2004). Consequently, $h = 2k$ or $h = k$ for even or odd scrolls, respectively, to avoid superimposing of the slopes because the plateaus can disappear. This process has been automated in (Muñoz-Pacheco & Tlelo-Cuautle, 2010; Sánchez-López et al., 2010)

Henceforth, α is restricted to 1, so that to implement multi-scrolls attractors using practical opamps one needs to scale the DRs from the SNLF (Lü et al., 2004). Then, the SNLF series is redefined by (8), where α allows that $k < 1$ because the chaos-condition now applies on the new slope $s = \frac{k}{\alpha}$. In this manner, k and α can be selected to permit $k < 1$, so that the DRs in (7) can be scaled. As a result, 6-scrolls attractors are generated with $a = b = c = d = 0.7, k = 1, \alpha = 6.4e^{-3}, s = 156.25, h = 2, p = q = 2$, as shown in Fig. 7b. Now, the DRs of the attractors are within the DRs of the real behavior of the opamps. Besides, it is possible to have small DRs depending on the values of k and α.

$$f(x;k,h,p,q) = \begin{cases} (2q+1)k & \text{if } x > qh+\alpha \\ \frac{k}{\alpha}(x-ih)+2ik & \text{if } \mid x-ih \mid \leq \alpha \\ & -p \leq i \leq q \\ (2i+1)k & \text{if } ih+\alpha < x < (i+1)h-\alpha \\ & -p \leq i \leq q-1 \\ -(2p+1)k & \text{if } x < -ph-\alpha \end{cases} \tag{8}$$

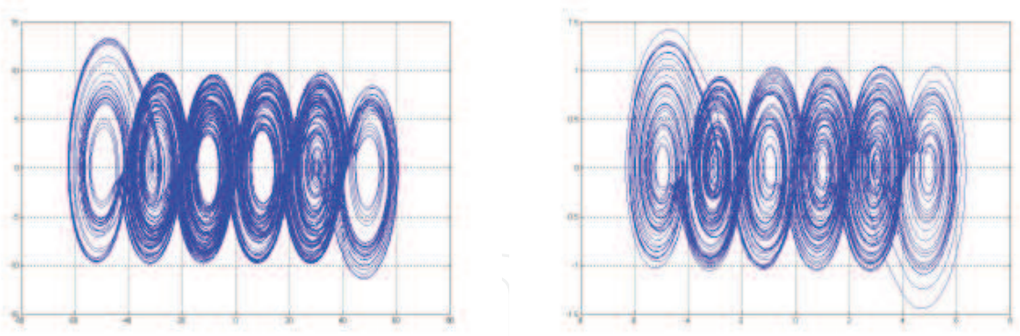

(a) (b)

Fig. 7. 6-scrolls attractors: (a) without DR scaling and (b) with DR scaling

3.2 Circuit realization

The dynamical system in (6) has the block diagram representation shown in Fig. 8, which is realized with 3 integrators and an adder. Each block can be realized with different kinds of active devices, namely: OpAmps, CFOAs, current conveyors (CC), unity-gain-cells (UGCs), and so on. The realization of the dynamical system in (6) using opamps is shown in Fig. 9 and by using CFOAs in Fig. 10.

By applying Kirchhoff's current-law in Fig. 10 one obtains (9), where $SNLF = i(x)R_{ix}$. The parameters are determined by (10).

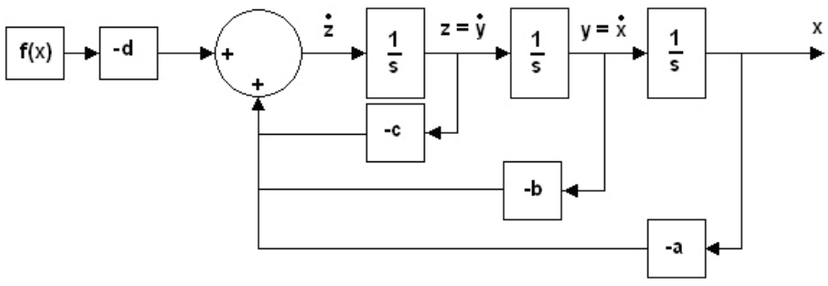

Fig. 8. Block diagram description of (6)

$$\begin{aligned} \frac{dx}{dt} &= \frac{y}{RC} \\ \frac{dy}{dt} &= \frac{z}{RC} \\ \frac{dz}{dt} &= -\frac{x}{R_xC} - \frac{y}{R_yC} - \frac{z}{R_{ix}C} + \frac{i(x)R_{ix}}{R_{ix}C} \end{aligned} \tag{9}$$

$$C = \frac{1}{0.7R_{ix}}, R_x = R_y = R_z = \frac{1}{0.7C}, R = \frac{1}{C} \tag{10}$$

The circuit realization of the SNLF in Fig. 9 and Fig. 10, can be implemented by using opamps and CFOAs, respectively working in the saturation region with shift bias-levels. For instance,

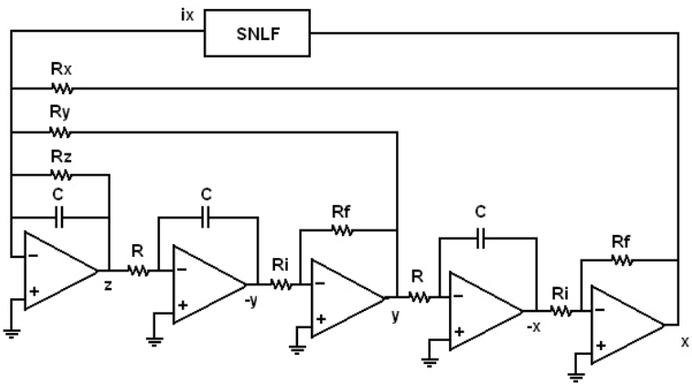

Fig. 9. OpAmp-based implementation of (6)

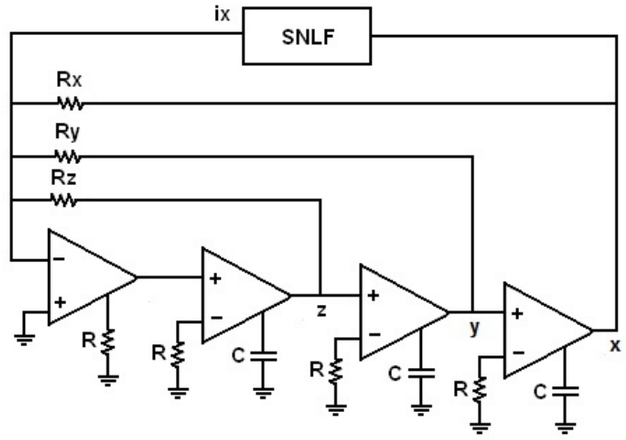

Fig. 10. CFOA-based implementation of (6)

the OpAmp and CFOA voltaje behaviors can be modeled by the opamp finite-gain model shown in Fig. 11 (Chen et al., 1995), so that a SNLF can be described by $V_o = \frac{A_v}{2}(\mid V_i + \frac{V_{sat}}{A_v} \mid - \mid V_i - \frac{V_{sat}}{A_v})$, and if a shift-voltage ($\pm E$) is added, as shown in Fig. 12, one gets the shifted-voltage SNLFs determined by (11) for positive and negative shifts, respectively. Now, $\alpha = V_{sat}/A_v$ are the breakpoints, $k = V_{sat}$ is the saturated plateau, and $s = V_{sat}/\alpha$ is the saturated slope. A resistor can be added to realize a current-to-voltage transformation, e.g. $i_o = V_o/R_c$.

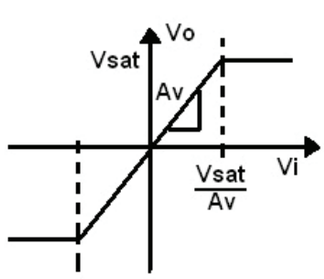

Fig. 11. OpAmp finite-gain model

To generate the SNLF (in Fig. 11), E takes different values in (11) to synthesize the required plateaus and slopes. The cell shown in Fig. 13a is used to realize voltage and current SNLFs from (11). The value of the plateaus k, in voltage and current modes, the breakpoints α, the slope and h are evaluated by (12) (Muñoz-Pacheco & Tlelo-Cuautle, 2008).

$$V_o = \frac{A_v}{2}(\mid V_i + \frac{V_{sat}}{A_v} - E \mid - \mid V_i - \frac{V_{sat}}{A_v} - E) \qquad V_o = \frac{A_v}{2}(\mid V_i + \frac{V_{sat}}{A_v} + E \mid - \mid V_i - \frac{V_{sat}}{A_v} + E) \tag{11}$$

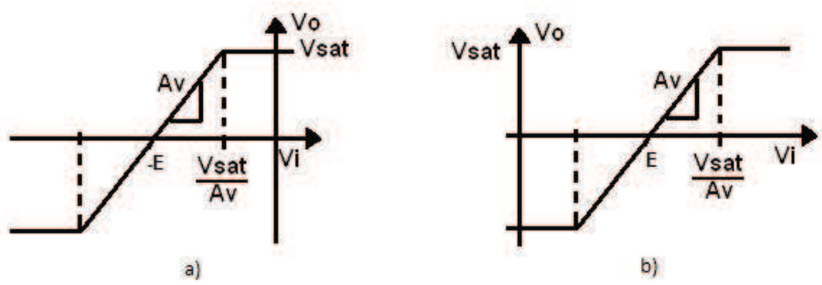

Fig. 12. SNLF shift-voltage (a) negative shift (b) positive shift

$$k = R_{ix} I_{sat}, \qquad I_{sat} = \frac{V_{sat}}{R_C}, \qquad \alpha = \frac{R_{iz} \mid V_{sat} \mid}{R_{fz}}, \qquad S = \frac{h}{\alpha}, \qquad h = \frac{E_i}{(1 + \frac{R_{iz}}{R_{fz}})} \tag{12}$$

For instance, the cell in Fig. 13 can realize the SNLF from (8), and the number of basic cells (BC) is determined by BC=(number of scrolls)-1, which are parallel-connected as shown in Fig. 14 (Muñoz-Pacheco & Tlelo-Cuautle, 2008).

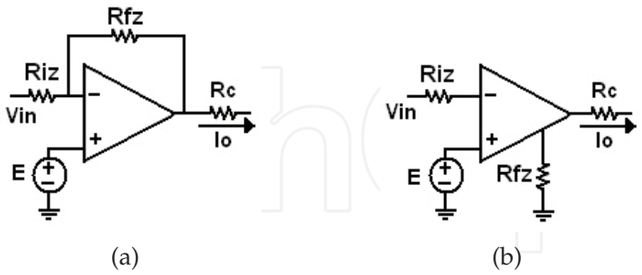

Fig. 13. Basic cell to generate SNLFs: (a) OpAmp implementation, (b) CFOA implementation

3.3 Multi-scroll attractors generation

The design automation of multi-scroll chaos generators for 1-3 dimensions can be found in (Muñoz-Pacheco & Tlelo-Cuautle, 2010). In this subsection we show the simulation using opamps. Experimental results using CFOAs and current conveyors can be found in (Trejo-Guerra, Sánchez-López, Tlelo-Cuautle, Cruz-Hernández & Muñoz-Pacheco, 2010) and (Sánchez-López et al., 2010), respectively.

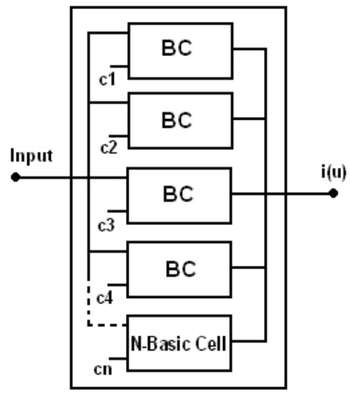

Fig. 14. Structure to synthesize SNLFs

By selecting funtional specifications: N=5-scrolls, F=10Khz and $EL = \pm 5V$, if $V_{sat} = \pm 6.4V$ (typical value for the commercially available OpAmp TL081 with $Vdd = \pm 8V$), the circuit synthesis result for 5 and 6- scrolls attractors are shown in Fig. 15 and Fig. 16. By setting $E_1 = \pm 1V, E_2 = \pm 3V, h_1 \cong 1, h_2 \cong 3$ to generate 5-scrolls; and $E_1 = \pm 2V, E_2 = \pm 4V, h_1 \cong 2, h_2 \cong 4$ to generate 6-scrolls; and $a = b = c = d = 0.7, k = 1, \alpha = 6.4e^{-3}, s = 156.25$, the circuit elements are: $R_{ix} = 10K\Omega, C = 2.2nf, R = 7K\Omega, R_x = R_y = R_z = 10K\Omega, R_f = 10K\Omega, R_i = 10K\Omega$ in (10) and $R_{ix} = 10K\Omega, R_c = 64K\Omega, R_{iz} = 1K\Omega, R_{fz} = 1M\Omega$ in (12).

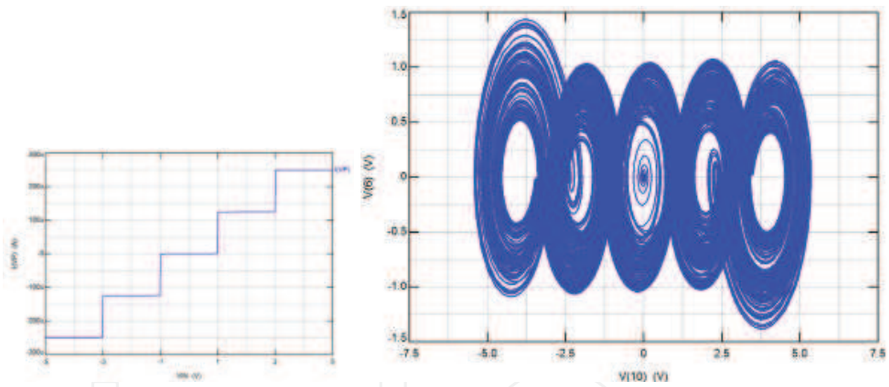

(a) SNLF (b) 5-scrolls attractor

Fig. 15. Generation of SNLF for 5-scrolls using opamps.

4. Realization of chaotic oscillators using current-feedback operational amplifiers

This section shows the simulation results for the SNLF based multi-scroll chaos generatos using CFOAs. Basically, from the results provided in the previos section, we can realize the circuit using CFOAs, instead of opamps. In this manner, by selecting funtional specifications: N=5-scrolls, F=10Khz and $EL = \pm 5V$, if $V_{sat} = \pm 6.4V$ (typical value for the coomercially available CFOA AD844 with $Vdd = \pm 10V$), the circuit simulation results for generating 5 and 6-scrolls attractors are shown in Fig. 17 and Fig. 18. Where $E_1 = \pm 1V, E_2 = \pm 3V, h_1 \cong 1, h_2 \cong 3$ to generate 5-scrolls; and $E_1 = \pm 2V, E_2 = \pm 4V, h_1 \cong 2, h_2 \cong 4$ to generate 6-scrolls; and $a = b = c = d = 0.7, k = 1, \alpha = 6.4e^{-3}, s = 156.25$, to calculate the circuit element values:

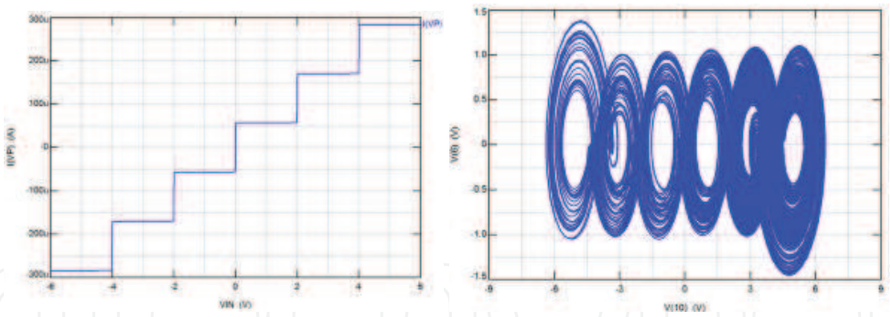

(a) SNLF (b) 6-scrolls attractor

Fig. 16. Generation of SNLF for 6-scrolls using opamps.

$R_{ix} = 10K\Omega, C = 2.2nf, R = 7K\Omega, R_x = R_y = R_z = 10K\Omega, R_f = 10K\Omega, R_i = 10K\Omega$ in (10), and $R_{ix} = 10K\Omega, R_c = 64K\Omega, R_{iz} = 1K\Omega, R_{fz} = 1M\Omega$ in (12).

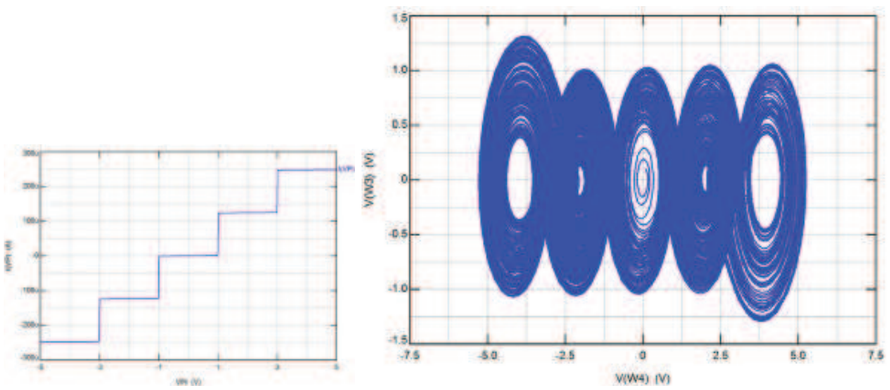

(a) SNLF (b) 5-scrolls attractor

Fig. 17. Generation of SNLF for 5-scrolls using CFOAs.

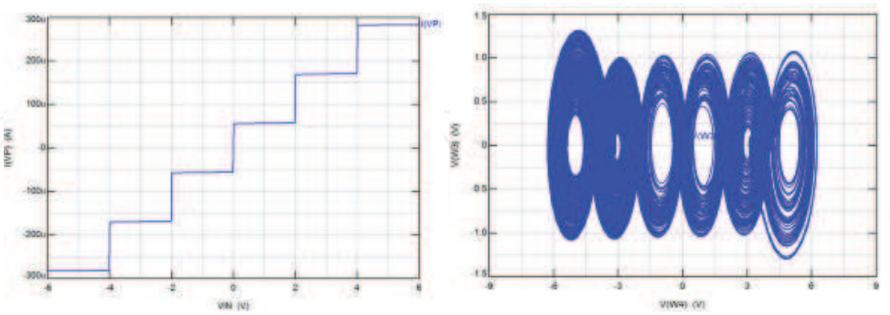

(a) SNLF (b) 6-scrolls attractor

Fig. 18. Generation of SNLF for 6-scrolls using CFOAs.

As one sees, the simulation results using CFOAs are quite similar to that using opamps. However, the electrical characteristics of the CFOA enhance the performance of the chaos generator, compared to opamp based circuit realizations. This advantage of the CFOA compared to the opamp is shown in the following section for the implementation of a secure communication system using multi-scroll chaos generators.

5. Synchronization of multi-scroll attractors

This section presents the synchronization using Hamiltonian forms and an observer approach (Sira-Ramírez & Cruz-Hernández, 2001). Let's consider the dynamical system described by the master circuit in (13). An slave system is a copy of the master and can be described by (14).

$$\dot{x} = F(x) \qquad \forall x \in \mathbb{R}^n \tag{13}$$

$$\dot{\xi} = F(\xi) \qquad \forall x \in \mathbb{R}^n \tag{14}$$

Definition: Two chaotic systems described by a set of states $x_1, x_2 \dots x_n$ (13) and $\xi_1, \xi_2 \dots \xi_n$ (14) will synchronize if the following limit fulfills (Shuh-Chuan et al., 2005; Sira-Ramírez & Cruz-Hernández, 2001):

$$\lim_{t \to \infty} \mid x(t) - \xi(t) \mid \equiv 0 \tag{15}$$

For any initial conditions $x(0) \neq \xi(0)$. Due to the real limitations of electronic devices, a tolerance value is used in practical applications, where there are some other agents like noise, distortion, component mismatching, etc.

$$\mid x(t) - \xi(t) \mid \leq \epsilon_t \qquad \forall t \geq t_f. \tag{16}$$

Where ϵ is the allowed tolerance value and a time $t_f < \infty$ is assumed. Equations (15) and (16) assume the synchronization error defined as

$$e(t) = x(t) - \xi(t) \tag{17}$$

5.1 Hamiltonian Synchronization Approach

To satisfy the condition in (15) and (17) between two systems, it is necessary to establish a physical coupling between them through which energy flows. If the energy flows in one direction between the systems, it is one-way coupling, known as master-slave configuration. This section is based on the work of (Sira-Ramírez & Cruz-Hernández, 2001). To synchronize two systems by applying Hamiltonian approach, their equations must be placed in the Generalized Hamiltonian Canonical form. Most of the well knew systems can fulfill this requirement, thus, the reconstruction of the state vector from a defined output signal will be possible attending to the observability or detectability of a pair of constant matrices.
Consider a class of Hamiltonian Forms with destabilizing vector field $F(y)$ and lineal output $y(t)$ of the form (18).

$$\dot{x} = J(y)\frac{\partial H}{\partial x} + (I + S)\frac{\partial H}{\partial x} + F(y), \qquad \forall x \in \Re^n; \qquad y = C\frac{\partial H}{\partial x}, \qquad \forall y \in \Re^n \tag{18}$$

Where I denotes a constant antisymmetric matrix; S denotes a symmetric matrix; the vector $y(t)$ is the system output and C is a constant matrix. The described system has an observer if one first considers $\xi(t)$ as the vector of the estimated states $x(t)$,when $H(\xi)$ is the observer's energy function. In addition $n(t)$ is the estimated output calculated from $\xi(t)$ and the gradient vector $\frac{\partial H(\xi)}{\partial \xi}$ is equal to $M\xi$ with M being a symmetric constant matrix positive definited. Then, for (18) a nonlinear observer with gain K is (19).

$$\dot{\xi} = J(y)\frac{\partial H}{\partial \xi} + (I+S)\frac{\partial H}{\partial \xi} + F(y) + K(y-\eta), \qquad \eta = C\frac{\partial H}{\partial \xi} \tag{19}$$

Where the state estimation error is naturally $e(t) = x(t) - \xi(t)$ and the system estimated error output is $e_y = y(t) - \eta(t)$, both described by the dynamical system (20).

$$\dot{e} = J(y)\frac{\partial H}{\partial e} + (I+S-KC)\frac{\partial H}{\partial e}, \qquad e \in \Re^n; \qquad e_y = C\frac{\partial H}{\partial e}, \qquad e_y \in \Re^m. \tag{20}$$

The following assumption has been made with some abuse of notation $\frac{\partial H(e)}{\partial e} = \frac{\partial H}{\partial x} - \frac{\partial H}{\partial \xi} = M(x-\xi) = Me$. Also, the equivalence $I + S = W$ will be assumed. To maintain stability and to guarantee the synchronization error convergence to zero, two theorems are taken into account.

THEOREM **1.** *(Sira-Ramírez & Cruz-Hernández, 2001). The state $x(t)$ of the system in the form (18) can be globally, asymptotically and exponentially estimated by the state $\xi(t)$ of an observer in the form (19), if the pair of matrix (C,W) or (C, S), are observable or at least detectable.*

THEOREM **2.** *(Sira-Ramírez & Cruz-Hernández, 2001). The state $x(t)$ of the system in the form (18) can be globally, asymptotically and exponentially estimated by the state $\xi(t)$ of an observer in the form (19), if and only if, a constant matrix K can be found to form the matrix $[W-KC] + [W-KC]^T = [S-K] + [S-KC]^T = 2[S - \frac{1}{2}(KC + C^T K^T)]$ which must be negative de□nite.*

In the successive, to find an observer for a system in the Hamiltonian form (18), the system will be arranged in the form (19), keeping observability or at least detectability and proposing a matrix $y(t)$ such that a gain matrix K can be found to achieve the conditions of Theorem 2.

5.2 Synchronization circuit implementation

Our proposed schemes for the synchronization of multi-scroll chaos systems of the form (19), by using CFOAs and OpAmps are shown in Fig.19 and Fig.20, respectively. The vector K in (19) is the observer gain and it is adjusted according to the sufficiency conditions for synchronization (Sira-Ramírez & Cruz-Hernández, 2001).
By selecting $R_{io} = 10k\Omega, R_{fo} = 3.9M\Omega$ and $R_{ko} = 22\Omega$ in Fig. 19 and Fig. 20, HSPICE simulation of the response of the synchronization whit OpAmps and CFOAs is shown in Fig. 21 and Fig. 24, respectively.
The synchronization error is shown in Fig. 22 and Fig. 25, which can be adjusted with the gain of the observer. The coincidence of the states is represented by a straight line with a unity-slope (identity function) in the phase plane of each state as shown in Fig. 23 and Fig. 26.

6. Experimental Synchronization results using CFOAs

The realization of Fig. 20 was done by using the commercially available CFOA AD844.

6.1 Generation of a 5-scrolls attractor

Figure 27 shows the experimental mesurement for the implementation of the 5-scrolls SNLF. By selecting $R_{ix} = 10K\Omega, C = 2.2nf, R = 7K\Omega, R_x = R_y = R_z = 10K\Omega, R_f = 10K\Omega, R_i = 10K\Omega$ in Fig. 20 and $R_{ix} = 10K\Omega, R_c = 64K\Omega, R_{iz} = 1K\Omega, R_{fz} = 1M\Omega, E_1 = \pm 1V$ and $E_2 = \pm 3V$ with $V_{sat} = +7.24V$ and $-7.28V$ in the BC (SNLF), the result is N=5-scrolls, F=10Khz, $EL = \pm 5V$ as shown in Fig. 28.

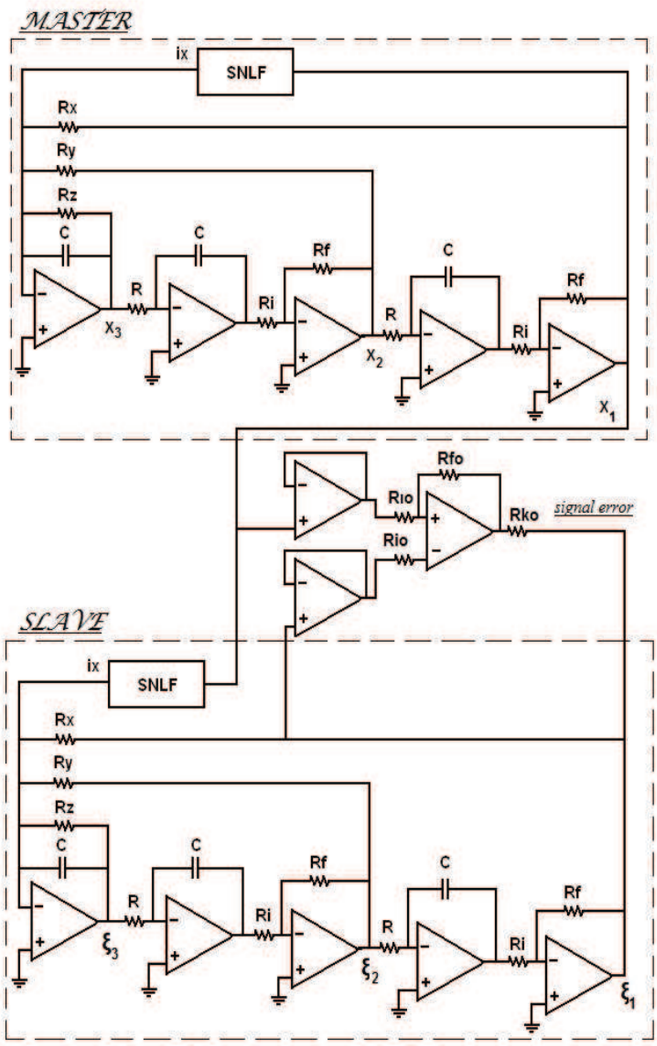

Fig. 19. Circuit realization for the synchronization using OpAmps

The synchronization result of Fig. 20 by selecting $R_{io} = 10k\Omega, R_{fo} = 3.9M\Omega$ and $R_{ko} = 3\Omega$ is shown in Fig. 29, the coincidence of the states is represented by a straight line with slope equal to unity in the phase plane for each state.

6.2 Chaotic system whit 6-scrolls attractor

Figure 30 shows the implementation of the 6-scrolls SNLF.
The synchronization result of Fig. 31 by selecting $R_{io} = 10k\Omega, R_{fo} = 3.9M\Omega$ and $R_{ko} = 3\Omega$ is shown in Fig. 32, the coincidence of the states is represented by a straight line with slope equal to unity in the phase plane for each state.

7. Chaos systems applied to secure communications

A communication system can be realized by using chaotic signals (Cruz-Hernández et al., 2005; Kocarev et al., 1992). Chaos masking systems are based on using the chaotic signal, broadband and look like noise to mask the real information signal to be transmitted, which

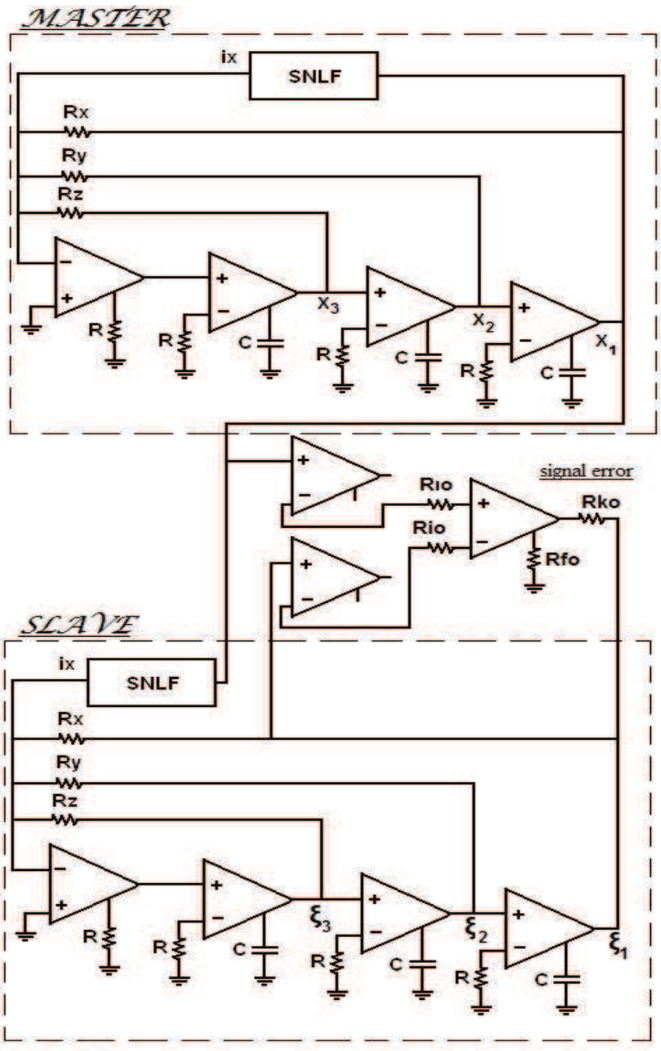

Fig. 20. Circuit realization for the synchronization using CFOAs

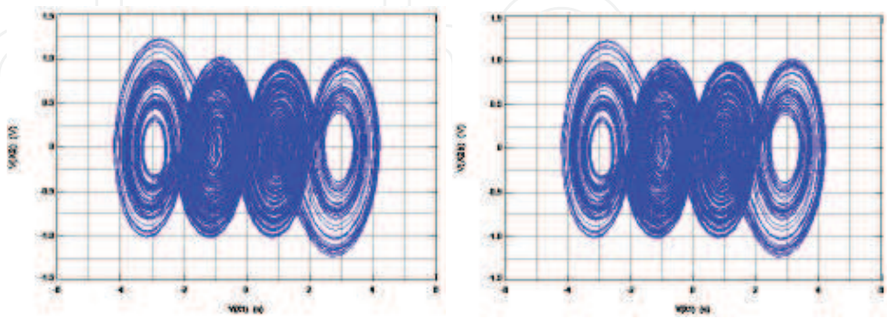

(a) master circuit (b) slave circuit

Fig. 21. Chaotic 4-scrolls atractor realized with OpAmps

may be analog or digital. One way to realize a chaos masking system is to add the information

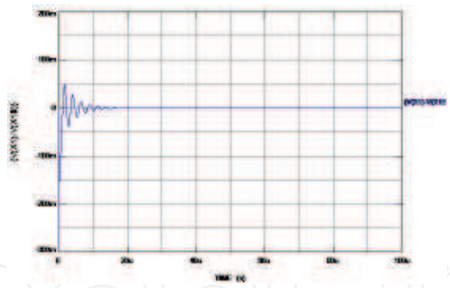

Fig. 22. Synchronization Error when using OpAmps

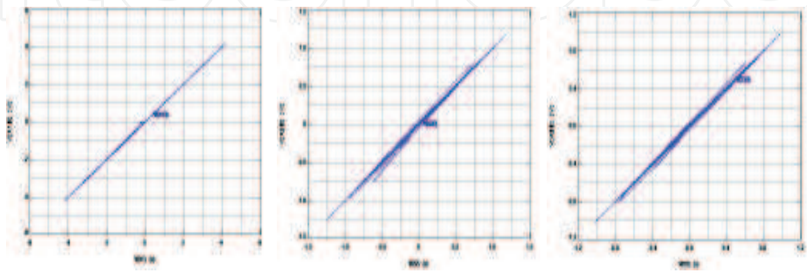

(a) (b) (c)

Fig. 23. Error phase-plane when using OpAmps

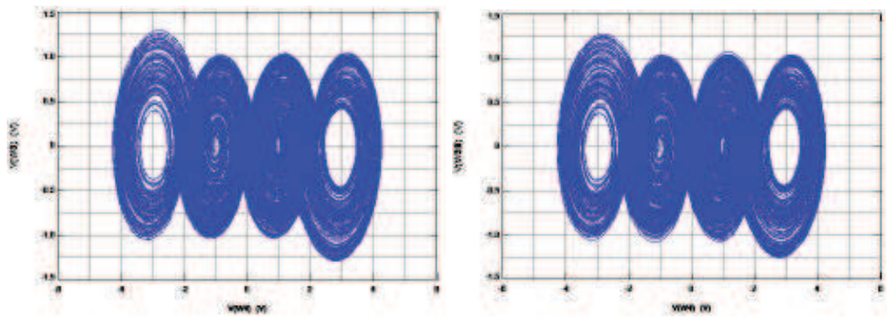

(a) master circuit (b) slave circuit

Fig. 24. Chaotic 4-scrolls atractor using CFOAs

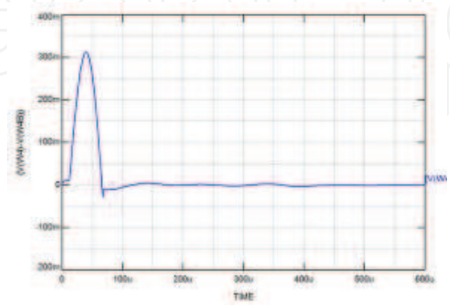

Fig. 25. Synchronization Error when using CFOAs

signal to the chaotic signal generated by an autonomous chaos system, as shown in Figure 33. The transmitted signal in this case is:

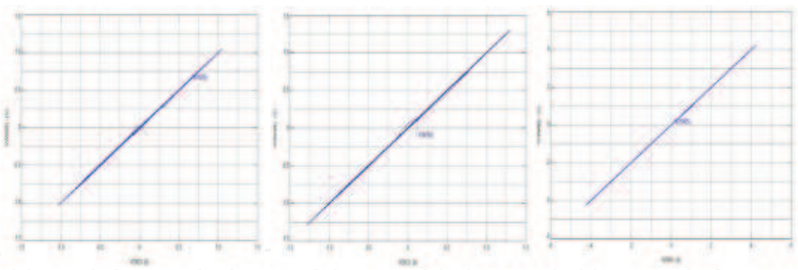

(a) (b) (c)

Fig. 26. Error phase plane when using CFOAs

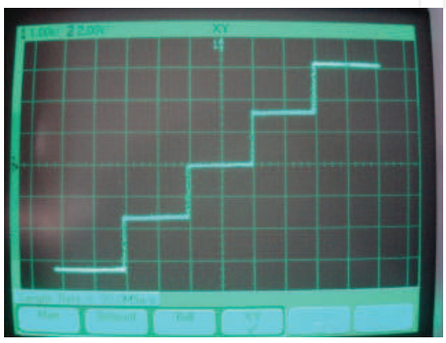

Fig. 27. 5-scrolls SNLF

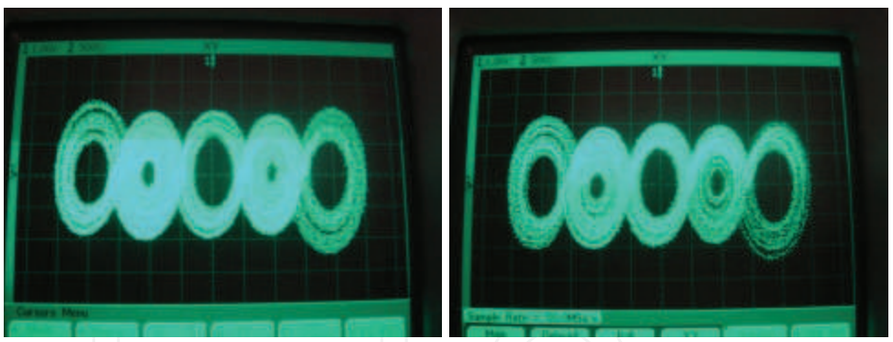

(a) master circuit (b) slave circuit

Fig. 28. Chaotic 5-scrolls attractor

$$\bar{y}(t) = y(t) + m(t) \tag{21}$$

where $m(t)$ is the signal information to be conveyed (the message) and $y(t)$ is the output signal of the chaotic system.

7.1 Two transmission channels

As illustrated in Fig. 34, this method is to synchronize the systems in master-slave configuration by a chaotic signal, $x_1(t)$, transmitted exclusively on a single channel, while to transmit a confidential message $m(t)$, it is encrypted with another chaotic signal, $x_2(t)$ by an additive process, this signal can be send through a second transmission channel.

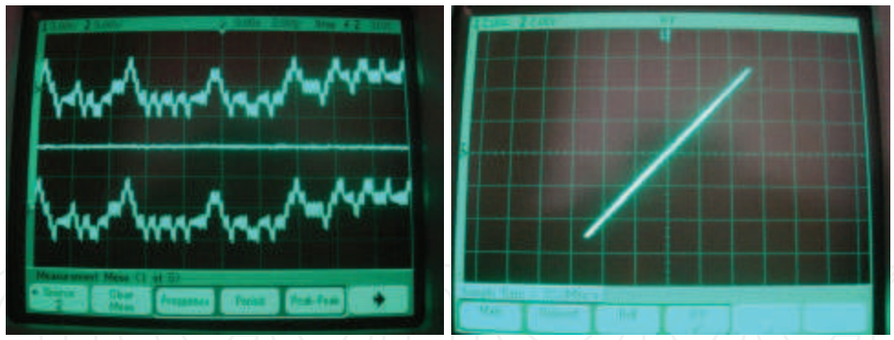

(a)

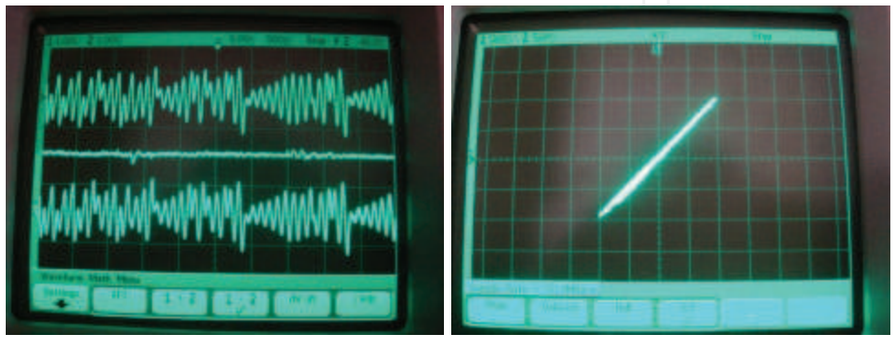

(b)

Fig. 29. Diagram in the phase plane and time signal (a) X_1vs ξ_1, (b) X_2 vs ξ_2

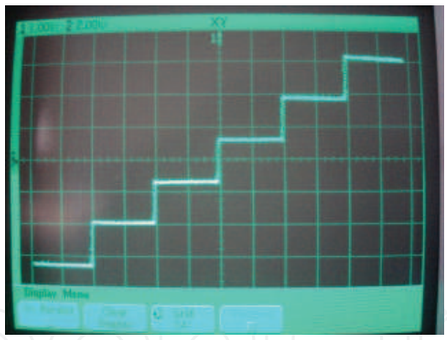

Fig. 30. 6-scrolls SNLF

Message recovery is performed by a reverse process, in this case, a subtraction to the signal received $\bar{y}(t) = x_2(t) + m(t)$, it is obvious that ywe want to subtract a chaotic signal identical to $x_2(t)$ for faithful recovery of the original message. It is important to note that there exists an error in synchrony given by $e_1(t) = x_1(t) - \hat{x}_1(t) = 0$, thus, $\hat{m}(t) = m(t)$.

7.2 Experimental results

We implemented an additive chaotic masking system using two transmission channels of the form (18), synchronized by Hamiltonian forms the receiver chaotic system is given by (19) , using the scenario of unidirectional master-slave coupling, as shown in Fig. 35.
The message to convey is a sine wave of frequency f = 10Khz and 500mV amplitude. Figures 36 and 37 show the experimental result of the secure transmission using chaos generators

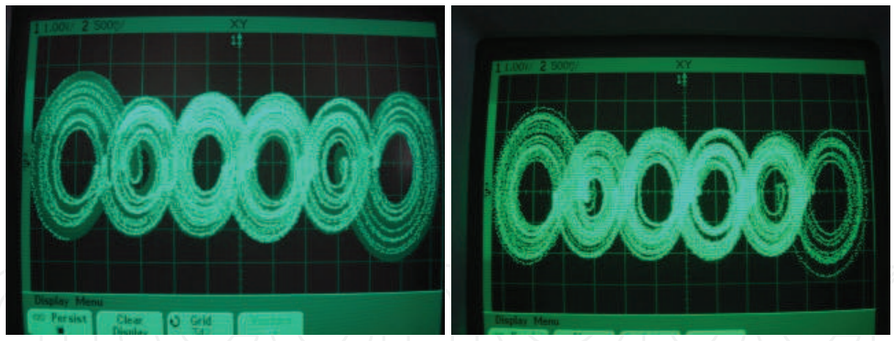

(a) master circuit (b) slave circuit

Fig. 31. Chaotic 6-scrolls attractor

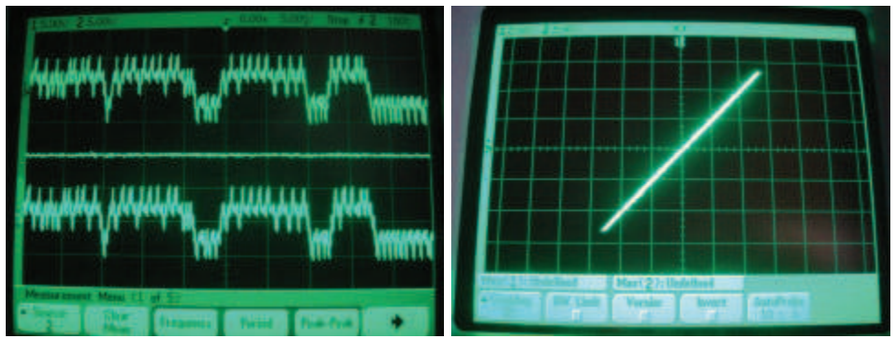

(a)

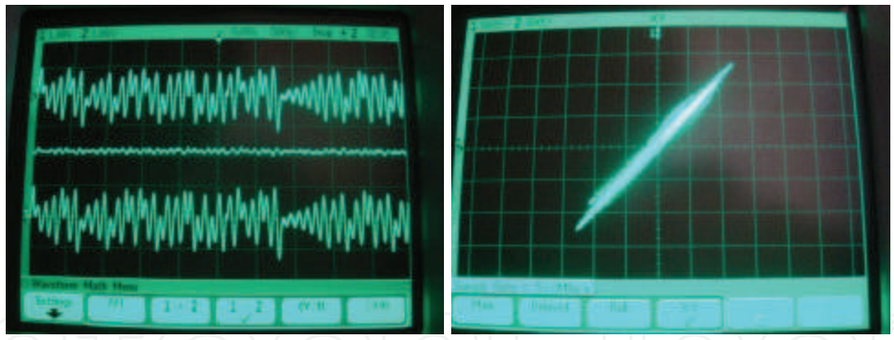

(b)

Fig. 32. Diagram in the phase plane and time signal (a) X_1vs ξ_1, (b) X_2 vs ξ_2

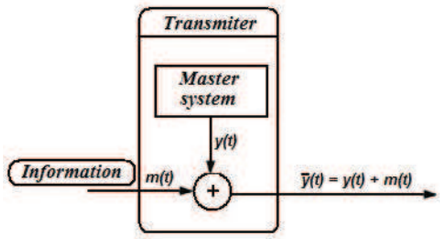

Fig. 33. Chaotic masking scheme

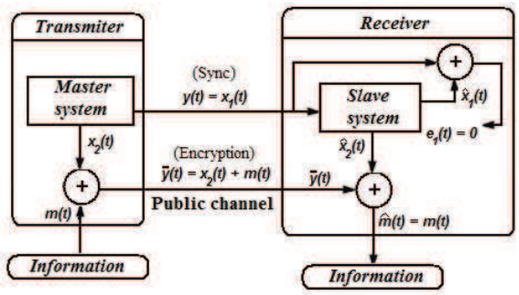

Fig. 34. Additive chaotic encryption scheme using two transmission channels

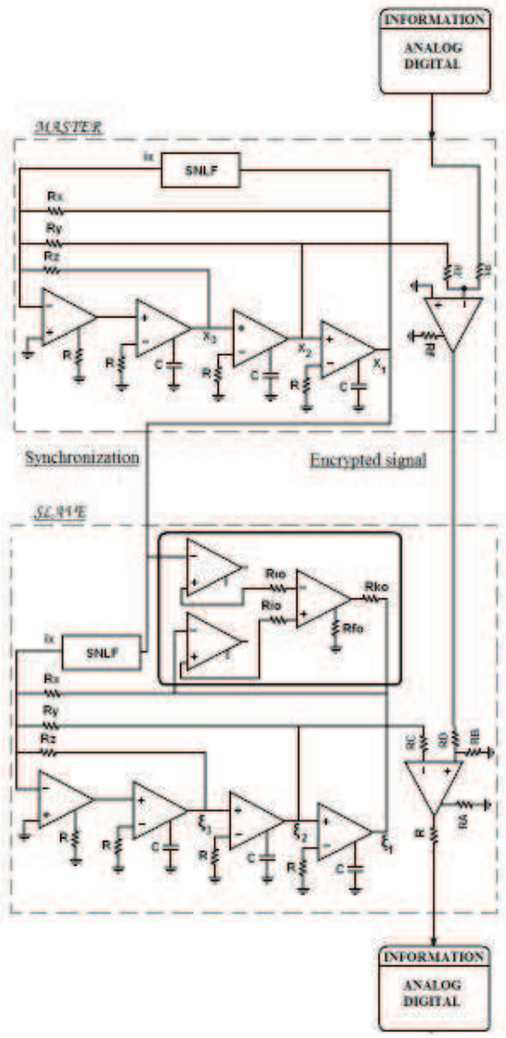

Fig. 35. Chaotic transmission system using CFOAs

of 5 and 6-scrolls, respectively. $m(t)$: confidential signal, $x_2(t) + m(t)$: encrypted signal transmitted by the public channel and $\hat{m}(t)$: reconstructed signal by the receiver.

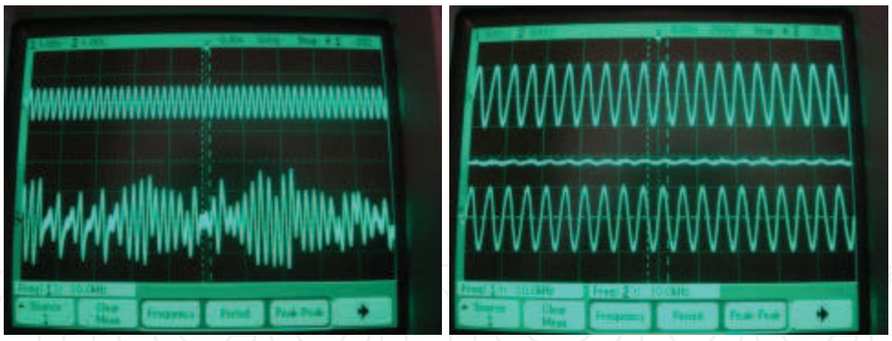

(a) (Ch1:1V/div; Ch2:1V/div).$Ch1 : m(t), Ch2 : x_2(t) + m(t)$ (b) (Ch1:500mV/div; Ch2:500mV/div; Center:500mV/div

Fig. 36. (a) Encryption of information, (b) Information retrieval

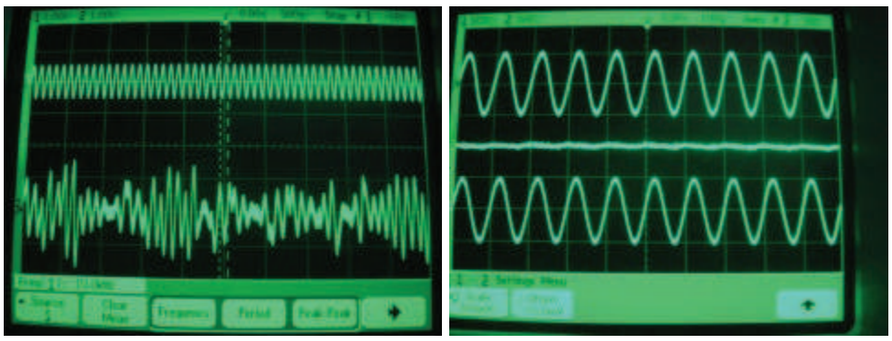

(a) (Ch1:1V/div; Ch2:1V/div) $Ch1 : m(t), Ch2 : x2_(t) + m(t)$ (b) (Ch1:500mV/div; Ch2:500mV/div; Center:500mV/div

Fig. 37. (a) Encryption of information, (b) Information retrieval

8. Conclusion

Chaos systems can be realized with almost every commercially available electronic device, and they can be designed with integrated circuit technology, for which there are many open problems regarding the number of scrolls to be generated, the bias levels to reduce power consumption, the increment in frequency response, tolerance to process and environment variations, and so on. Furthermore, the performances of the chaos systems will depend on the electrical characteristics of the devices. In this chapter we presented the design of chaos systems using commercially available devices such as the opamp and CFOA AD844.
We described how to generate multi-scroll attractors and how to realize the circuitry for the chaotic oscillator based on SNLFs.
The application of the designed chaos generators to a communication system was highlighted through experimental results using CFOAs. Open problems can also be related to the development of applications by using chaos systems with different number of scrolls and dimensions and with different kinds of chaos system topologies.

Acknowledgment

The first author thanks the support of the JAE-Doc program of CSIC, co-funded by FSE, of Promep-México under the project UATLX-PTC-088, and by Consejeria de Innovacion Ciencia

y Empresa, Junta de Andalucia, Spain, under the project number TIC-2532. The second author thanks the support from Promep-México under the project UPPUE-PTC-033. The last author thanks the CONACyT grant for his sabbatical stay at University of California at Riverside, during 2009-2010.

9. References

Castro-López, R., Fernández, F., Guerra-Vinuesa, O. & Rodriguez-Vazquez, A. (2006). *Reuse-Based Methodologies and Tools in the Design of Analog and Mixed-Signal Integrated Circuits*, Springer Publishers.

Chakraborty, S. & Dana, S. (2010). Shil'nikov chaos and mixed-mode oscillation in chua circuit, *Chaos* 20(2): 023107.

Chen, W., Vandewalle, J. & Vandenberghe, L. (1995). Piecewise-linear circuits and piecewiselinear analysis: Circuits and filters handbook, *CRC Press/IEEE Press* .

Chua, L. (1975). *Computer-Aided Analysis of Electronic Circuits: Algorithms and Computational Techniques*, Prentice Hall.

Cook, P. (1994). *Nonlinear Dynamical Systems*, Prentice Hall.

Cruz-Hernández, C., López-Mancilla, D., García-Gradilla, V., Serrano-Guerrero, H. & nez Pérez, R. N. (2005). Experimental realization of binary signals transmission using chaos, *J. Circuits Syst. Comput.* 14: 453–468.

Deng, W. (2007). Generating 3-D scroll grid attractors of fractional differential systems via stair function, *International Journal of Bifurcations and Chaos* 17(11): 3965–3983.

Dieci, L. (2002). Jacobian free computation of lyapunov exponents, *J. Dynam. Differ. Equat.* 14(3): 697–717.

Elhadj, Z. & Sprott, J. (2010). Generating 3-scroll attractors from one chua circuit, *International Journal of Bifurcations and Chaos* 20(1): 135–144.

Ergun, S. & Ozoguz, S. (2010). Truly random number generators based on non-autonomous continuous-time chaos, *International Journal of Circuit Theory and Applications* 38: 1–24.

Gámez-Guzmán, L., Cruz-Hernández, C., López-Gutiérrez, R. & García-Guerrero, E. (2008). Synchronization of multi-scroll chaos generators: Application to private communication, *Rev. Mexicana Fís.* 54(4): 299–305.

Kocarev, L., Halle, K. S., Eckert, K., Chua, L. O. & Parlitz, U. (1992). Experimental demonstration of secure communications via chaotic synchronization, *International Journal of Bifurcations and Chaos* 2(3): 709–713.

Kundert, K. (2004). *The Designer's Guide to Verilog-AMS*, Kluwer Academic Publishers.

Lin, Z. H. & Wang, H. X. (2010). Efficient image encryption using a chaos-based PWL memristor, *IETE Technical Review* 27(4): 318–325.

Lü, J., Chen, G., Yu, X. & Leung, H. (2004). Design and analysis of multiscroll chaotic attractors from saturated function series, *IEEE Trans. Circuits Syst. I* 51(12): 2476–2490.

Lu, J., Yang, G., Oh, H. & Luo, A. (2005). Chaos computing lyapunov exponents of continuous dynamical systems: method of lyapunov vectors, *Chaos, Solitons & Fractals* 23: 1879–1892.

Muñoz-Pacheco, J. & Tlelo-Cuautle, E. (2008). Synthesis of n-scroll attractors using saturated functions from high-level simulation, *Journal of Physics-Conference Series* (2nd Int. Symposium on Nonlinear Dynamics).

Muñoz-Pacheco, J. & Tlelo-Cuautle, E. (2009). Automatic synthesis of 2D-n-scrolls chaotic systems by behavioral modeling, *Journal of Applied Research and Technology* 7(1): 5–14.

Muñoz-Pacheco, J. & Tlelo-Cuautle, E. (2010). *Electronic design automation of multi-scroll chaos generators*, Bentham Sciences Publishers Ltd.

Ott, E. (1994). *Chaos in Dynamical systems*, Cambridge University Press.

Ramasubramanian, K. & Sriram, M. (2000). A comparative study of computation of lyapunov spectra with different algorithms, *Phys. Nonlinear Phenom.* 139: 72–86.

Sánchez-López, C., Castro-López, A. & Pérez-Trejo, A. (2008). Experimental verification of the Chua's circuit designed with UGCs, *IEICE Electron. Express* 5: 657–661.

Sánchez-López, C., Trejo-Guerra, R., Muñoz-Pacheco, J. & Tlelo-Cuautle, E. (2010). N-scroll chaotic attractors from saturated functions employing CCII+s, *Nonlinear Dynamics* 61(1-2): 331–341.

Sánchez-Sinencio, E. & Silva-Martínez, J. (2000). Cmos transconductance amplifiers, architectures and active filters: a tutorial, *IEE Proceedings- Circuits, Devices and Systems* 147(1): 3–12.

Sedra, A. & Smith, K. (1970). A second-generation current conveyor and its applications, *IEEE Trans. Circuit Th.* 17: 132–134.

Senani, R. & Gupta, S. (1998). Implementation of Chua's chaotic circuit using current feedback opamps, *Electron. Lett.* 34: 829–830.

Shuh-Chuan, T., Chuan-Kuei, H., Wan-Tai, C. & Yu-Ren, W. (2005). Synchronization of chua chaotic circuits with application to the bidirectional secure communication systems, *International Journal of Bifurcations and Chaos* 15(2): 605–616.

Sira-Ramírez, H. & Cruz-Hernández, C. (2001). Synchronization of chaotic systems: A generalized hamiltonian systems approach, *International Journal of Bifurcations and Chaos* 11(5): 1381–1395.

Strogatz, S. H. (2001). *Nonlinear Dynamics And Chaos: With Applications To Physics, Biology, Chemistry, And Engineering*, Westview Press.

Suykens, J., Huang, A. & Chua, L. (1997). A family of n-scroll attractors from a generalized chua's circuit, *International Journal of Electronics and Communications* 51(3): 131–138.

Tlelo-Cuautle, E. & C. Sánchez-López, D. M.-F. (2010). Symbolic analysis of (MO)(I)CCI(II)(III)-based analog circuits, *International Journal of Circuit Theory and Applications* 38(6): 649–659.

Tlelo-Cuautle, E., Gaona-Hernández, A. & Garcia-Delgado, J. (2006). Implementation of a chaotic oscillator by designing chua's diode with CMOS CFOAs, *Analog Integrated Circuits and Signal Processing* 48(2): 159–162.

Tlelo-Cuautle, E. & Munoz-Pacheco, J. (2007). Numerical simulation of chua's circuit oriented to circuit synthesis, *International Journal of Nonlinear Sciences and Numerical Simulation* 8(2): 249–256.

Trejo-Guerra, R., Sánchez-López, C., Tlelo-Cuautle, E., Cruz-Hernández, C. & Muñoz-Pacheco, J. (2010). Realization of multiscroll chaotic attractors by using current-feedback operational amplifiers, *Revista Mexicana de Física* 56(4): 268–274.

Trejo-Guerra, R., Tlelo-Cuautle, E., Cruz-Hernández, C. & Sánchez-López, C. (2009). Chaotic communication system using chua's oscillators realized with CCII+s, *Int. J. Bifurc. Chaos* 19(12): 4217–4226.

Trejo-Guerra, R., Tlelo-Cuautle, E., Jiménez-Fuentes, M. & Sánchez-López, C. (2010). Multiscroll oscillator based on floating gate cmos inverter, *Proceedings of the International Conference on Electrical Engineering, Computing Science and Automatic Control*, IEEE, Tuxtla Gutiérrez, pp. 541 – 545.

Trejo-Guerra, R., Tlelo-Cuautle, E., Muñoz-Pacheco, J., Cruz-Hernández, C. & Sánchez-López, C. (2010). Operating characteristics of mosfets in chaotic oscillators, *in* B. M. Fitzgerald (ed.), *Transistors: Types, Materials and Applications*, NOVA Science Publishers Inc.

Varrientos, J. & Sanchez-Sinencio, E. (1998). A 4-D chaotic oscillator based on a differential hysteresis comparator, *IEEE Trans. on Circuits and Systems I* 45(1): 3–10.

Yalçin, M., Suykens, J. & Vandewalle, J. (2002). Families of scroll grid attractors, *International Journal of Bifurcation and Chaos* 12(1): 23–41.

Yalcin, M., Suykens, J. & Vandewalle, J. (2000). Experimental confirmation of 3- and 5-scroll attractors from a generalized chua's circuit, *IEEE Trans. Circuits Syst.-I* 47: 425–429.

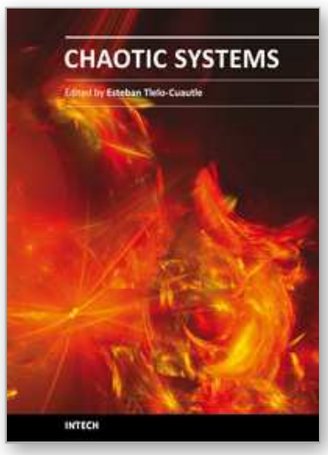

Chaotic Systems

Edited by Prof. Esteban Tlelo-Cuautle

ISBN 978-953-307-564-8
Hard cover, 310 pages
Publisher InTech
Published online 14, February, 2011
Published in print edition February, 2011

This book presents a collection of major developments in chaos systems covering aspects on chaotic behavioral modeling and simulation, control and synchronization of chaos systems, and applications like secure communications. It is a good source to acquire recent knowledge and ideas for future research on chaos systems and to develop experiments applied to real life problems. That way, this book is very interesting for students, academia and industry since the collected chapters provide a rich cocktail while balancing theory and applications.

InTech Europe
University Campus STeP Ri
Slavka Krautzeka 83/A
51000 Rijeka, Croatia
Phone: +385 (51) 770 447
Fax: +385 (51) 686 166
www.intechopen.com

InTech China
Unit 405, Office Block, Hotel Equatorial Shanghai
No.65, Yan An Road (West), Shanghai, 200040, China
中国上海市延安西路65号上海国际贵都大饭店办公楼405单元
Phone: +86-21-62489820
Fax: +86-21-62489821

IntechOpen